

# **Supplementary Information**

## **Quantitative Insights for Diagnosing Performance Bottlenecks in Lithium-Sulfur Batteries**

Saurabh Parab<sup>1</sup>, Jonathan Lee<sup>2</sup>, Matthew Miyagishima<sup>2</sup>, Qiushi Miao<sup>2</sup>, Bhargav Bhamwala<sup>2</sup>, Alex Liu<sup>2</sup>, Louis Ah<sup>2</sup>, Bhagath Sreenarayanan<sup>2</sup>, Kun Ryu<sup>3</sup>, Mingqian Li<sup>3</sup>, Neal Arakawa<sup>4</sup>, Robert Schmidt<sup>5</sup>, Mei Cai<sup>5</sup>, Fang Dai<sup>5</sup>, Ping Liu<sup>1,2</sup>, Shen Wang<sup>2,\*</sup>, Ying Shirley Meng<sup>2,3,\*</sup>

1 Materials Science and Engineering Program, University of California San Diego, La Jolla, CA, USA.

2 Aiso Yufeng Li Family Department of Chemical and Nano Engineering, University of California San Diego, La Jolla, CA, USA.

3 Pritzker School of Molecular Engineering, University of Chicago, Chicago, IL, USA.

4 Environmental and Complex Analysis Laboratory, University of California San Diego, La Jolla, CA, USA.

5 General Motors Research and Development Center, Warren, MI, USA.

\*Email: shw117@ucsd.edu; shirleymeng@uchicago.edu

## Table of Contents

### Discussion Sessions

1. HUGS Method Validation
  - a. HPLC-APCI-MS based peak assignment
  - b. Quantification using the semi-preparative HPLC-UV fractions
  - c. Quantification using the external standard
  - d. HPLC-UV Resolution Comparison
2. Dr. HUGS<sup>®</sup> Software
3. CS Cathode
  - a. Characterizations of CS
  - b. Special cases in CS batteries
  - c. HATN Cathode
  - d. CS Pouch Cells
4. SPAN Cathode
  - a. Characterizations of SPAN
  - b. Special cases in SPAN batteries

### Supplementary Figures

- S1. Determining the peak positions of  $\text{Me}_2\text{S}_x$  ( $3 < x < 9$ ) and  $\text{S}_8$  using HPLC-APCI-MS.
- S2. Quantification of  $\text{Me}_2\text{S}_x$  ( $4 \leq x \leq 8$ ) and  $\text{S}_8$  using Semi-preparative HPLC-UV.
- S3. Quantification of  $\text{Me}_2\text{S}_3$  using external standards by semi-preparative HPLC-UV.
- S4. HUGS Method Validation.
- S5. HUGS capacity retention pie plot.
- S6. Dr. HUGS<sup>®</sup> software for automated data processing of HUGS characterization.
- S7. CS battery charge-discharge curves in different cycling regions.
- S8. Cryo-FIB images and EDX mapping for cycled CS cathode top surface in different regions.
- S9. Cryo-FIB SEM images and EDX mapping for the cross-section of C-S Cathodes in different cycling regions.
- S10.  $\text{LiNO}_3$  consumption is shown through HPLC-UV Chromatography.
- S11. CS HUGS capacity storage plot with individual species.
- S12. CS battery at 1<sup>st</sup> discharge.
- S13. HUGS analysis for CS cathode special cases.

- S14. HUGS analysis results for HATN cathode.
- S15. CS pouch cell charge-discharge curves and the cycling performance in (a-b) constant gap and (c-d) 30 psi constant pressure setups.
- S16. Pouch cell HUGS capacity storage plot with individual species.
- S17. XPS analysis of SPAN cathode before and after soaking in DME.
- S18. Characterizations of Li-S Batteries with SPAN cathodes at Different Cycling Regions.
- S19. Cryo-FIB images and EDX mapping for cycled SPAN cathode top surface in different regions.
- S20. Cryo-FIB SEM images and EDX mapping for the cross-section of SPAN Cathodes in different cycling regions.
- S21. Cryo-FIB SEM top surface and cross-section images and SEM images of cross-section images of Li anodes from cycled SPAN batteries in different cycling regions.
- S22. SPAN HUGS capacity storage plot with each species.
- S23. HUGS analysis for Li-SPAN battery cycled at different C-rates.

### **Supplementary Tables**

Table S1. Calibration Curve Fitting Parameters.

Table S2. Precision and accuracy in Sulfur quantification by HPLC-UV.

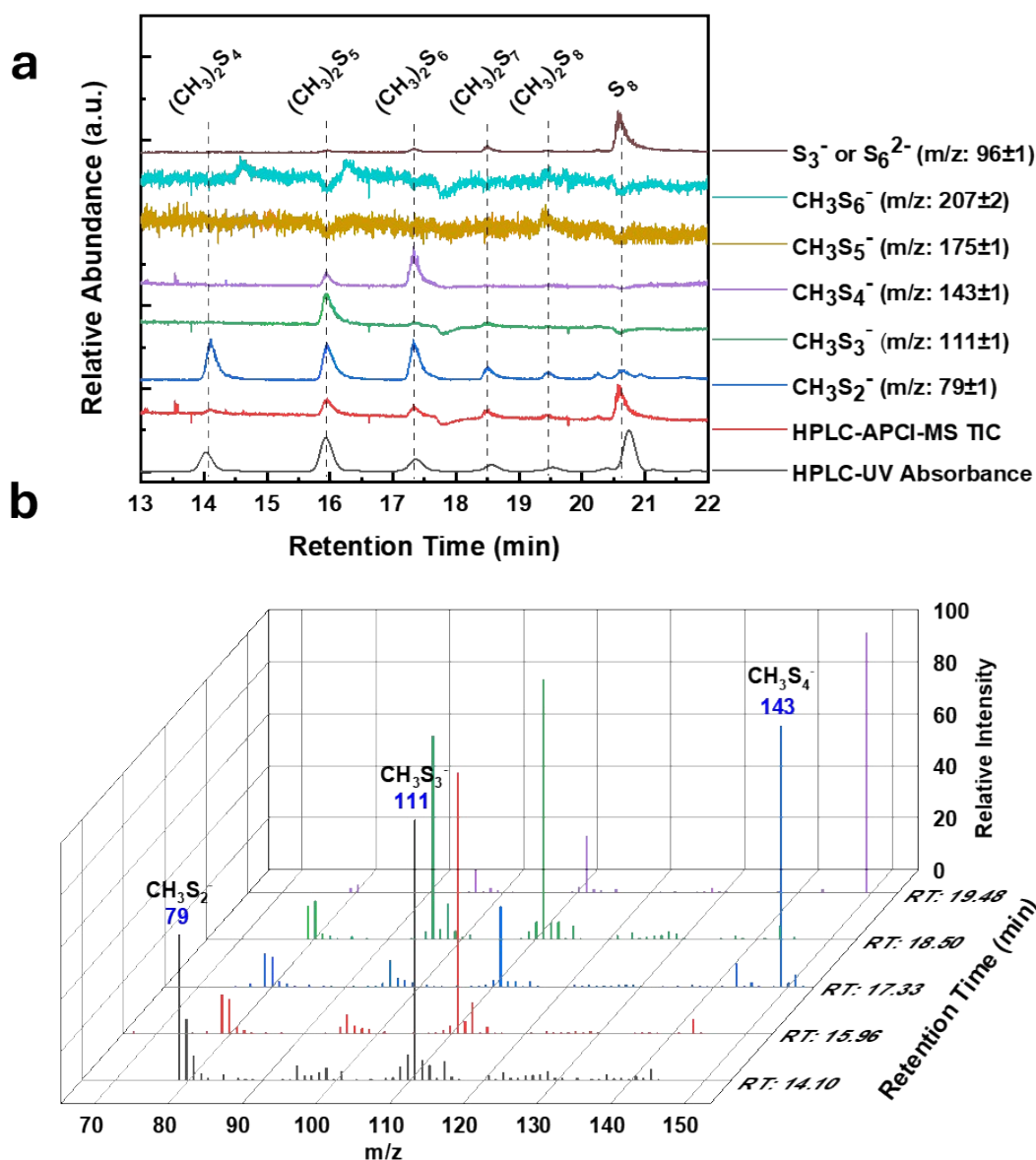
Table S3. Resolution parameters comparison between Semi-preparative and Analytical HPLC columns.

Table S4. Activity of the species in Li-S batteries at fully charged state.

Table S5. Dataset comparing the HUGS method with other reported methods in the literature with references.

## **1. HUGS Method Validation**

## 1.a. HPLC-APCI-MS based peak assignment



**Figure S1. Determining the peak positions of  $Me_2S_x$  ( $3 < x < 9$ ) and  $S_8$  using HPLC-APCI-MS.** **a.** Total ion chromatogram (TIC) and the ion chromatograms for  $m/z=79$  ( $CH_3S_2^-$ ),  $m/z=111$  ( $CH_3S_3^-$ ),  $m/z=143$  ( $CH_3S_4^-$ ),  $m/z=175$  ( $CH_3S_5^-$ ),  $m/z=207$  ( $CH_3S_6^-$ ), and  $m/z=96$  ( $S_6^{2-}$  or  $S_3^-$ ) obtained using HPLC-APCI-MS and UV-absorbance chromatogram obtained by HPLC-UV for comparison. **b.** Intensities of ions of  $m/z$  ranging from 70 to 150 at the fixed retention times corresponding to the peak positions of methylated species obtained using HPLC-APCI-MS. Intensities corresponding to anionic fragments of  $CH_3S_2^-$ ,  $CH_3S_3^-$ , and  $CH_3S_4^-$  are highlighted.

By collecting HPLC-UV absorbance data on derivatized polysulfides and mapping it with HPLC-APCI-MS data, we could confirm the positions of polysulfides and Sulfur (Figure

S1a). The long-chain methylated species are broken down into short-chain anionic fragments, as seen in Figure S1b).

### 1.b. Quantification using the semi-preparative HPLC-UV fractions

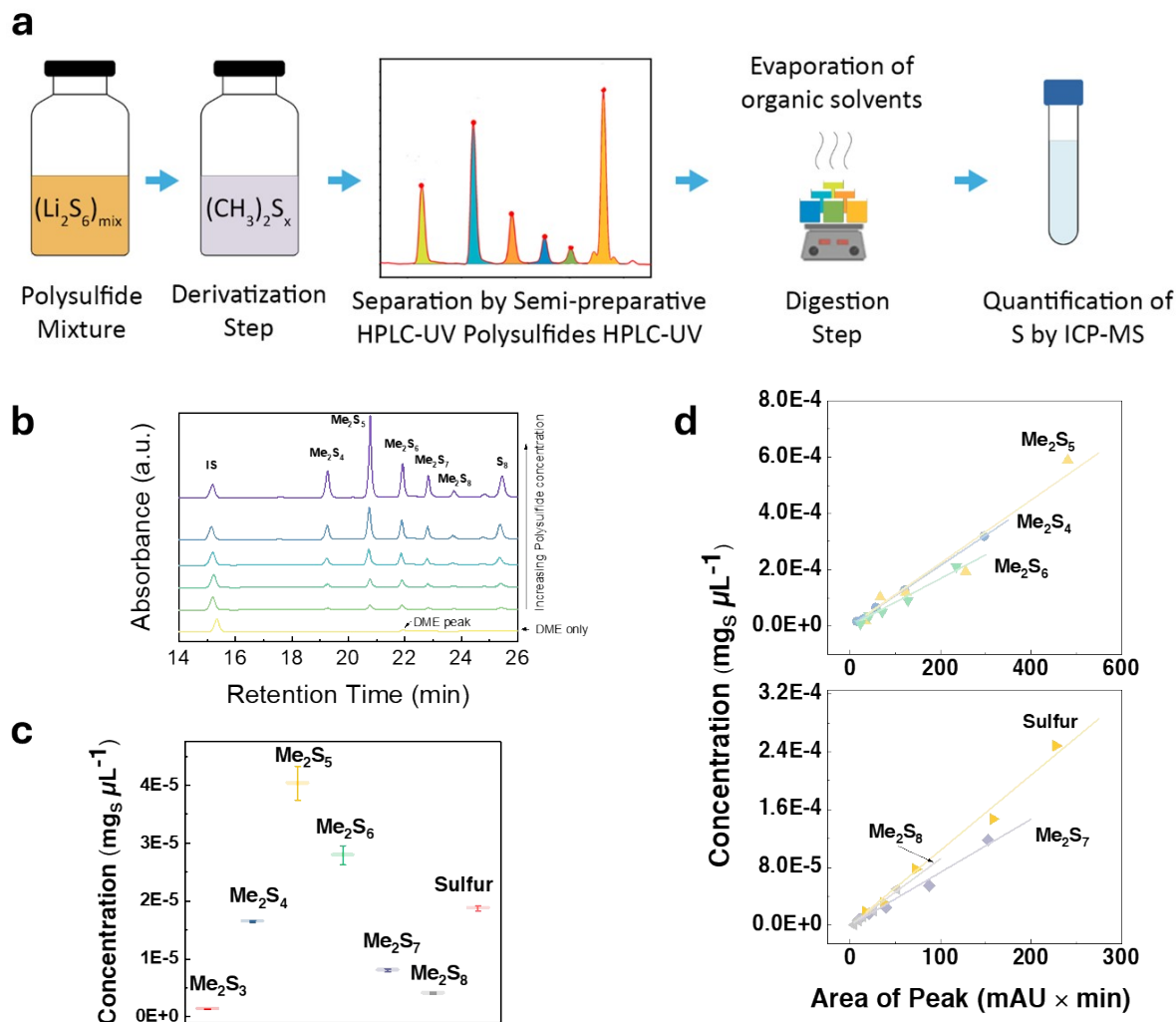


**Figure S2. Quantification of  $\text{Me}_2\text{S}_x$  ( $4 \leq x \leq 8$ ) and  $\text{S}_8$  using Semi-preparative HPLC-UV.** **a.** Process flow chart of derivatization, separation, fraction collection, digestion, and quantification of Sulfur in the digested solution by ICP-MS- $\text{O}_2$  reaction mode. **b.** HPLC-UV absorbance chromatograms of samples used to prepare calibration curves. **c.** The detection limits for each species. **d.** Linear fitting of calibration data points obtained by peak area from Semi-preparative HPLC-UV and concentration of the Sulfur in it by ICP-MS for each  $\text{Me}_2\text{S}_x$  ( $4 \leq x \leq 8$ ) and  $\text{S}_8$ .

Polysulfide solutions can be quenched by derivatizing their methylated form. These relatively stable methylated species can then be separated using a semipreparative column. The fractions of each polysulfide containing water and methanol from the solvent

gradient of HPLC can then be heated in a highly oxidizing environment of Nitric Acid and  $\text{H}_2\text{O}_2$  (1:1 v/v, 4 mL) at 180°C. The solution was topped up with 1% nitric acid matrix solution to perform triple quad ICP-MS- $\text{O}_2$  to quantify Sulfur in each species. The schematic of the process is shown in Figure S2a. The chromatograms of five derivatized polysulfide solutions are shown in Figure S2b. The detection limits for each species and their calibration curves are shown in Figures S2c and S2d, respectively.

### 1.c. Quantification using the external standard

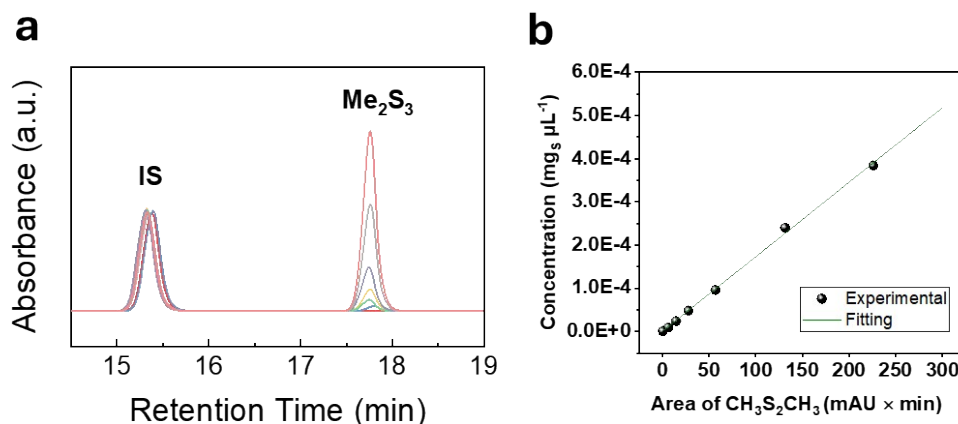


**Figure S3. Quantification of Me<sub>2</sub>S<sub>3</sub> using external standards by semi-preparative HPLC-UV. a.** HPLC-UV absorbance data and **b.** the calibration curve.

**Table S1. Calibration Curve Fitting Parameters**

Species	R <sup>2</sup>	Concentration (mg <sub>s</sub> μL <sup>-1</sup> )/Area
Me <sub>2</sub> S <sub>3</sub>	0.999	1.727E-6 ± 2.227E-8
Me <sub>2</sub> S <sub>4</sub>	0.999	1.076E-6 ± 1.344E-8
Me <sub>2</sub> S <sub>5</sub>	0.969	1.119E-6 ± 1.004E-7
Me <sub>2</sub> S <sub>6</sub>	0.989	8.440E-7 ± 4.552E-8
Me <sub>2</sub> S <sub>7</sub>	0.992	7.334E-7 ± 3.359E-8
Me <sub>2</sub> S <sub>8</sub>	0.988	9.213E-7 ± 5.014E-8
Sulfur	0.995	1.039E-6 ± 3.825E-8

**Table S2. Precision and accuracy in Sulfur quantification by HPLC-UV**

<b>Sample #</b>	<b>HPLC Area (mAU*min)</b>	<b>Sulfur concentration by Calibration Curve (mg/uL)</b>	<b>%Error</b>
1	170.517	177.17	-3.71
2	171.272	177.95	-4.17
3	170.969	177.64	-3.98
4	169.487	176.10	-3.08

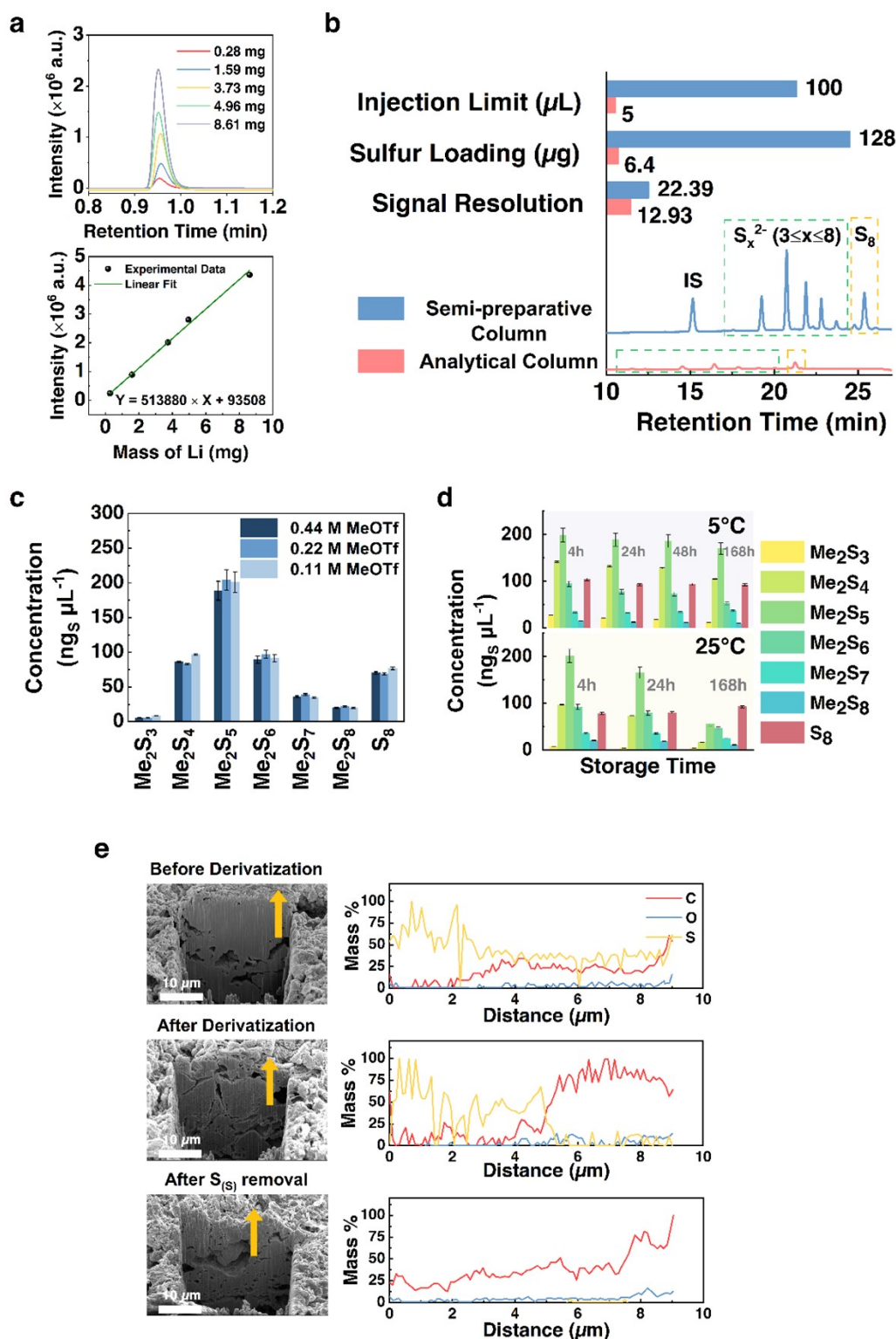


**Figure S4. HUGS Method Validation.** **a.** Chromatograms corresponding to standard samples of titration GC and calibration curve for  $\text{Li}^0$  quantification; **b.** Comparative parameters between semi-preparative and analytical HPLC columns for polysulfides and  $\text{S}_8$  quantification; **c.** Effect of different concentrations of methylation agent on the



quenching of polysulfide conversion equilibrium; **d.** Stability test of methylated-polysulfide solutions at different storage temperatures and durations **e.** Cryogenic Focused Ion Beam Scanning Electron Microscopy (Cryo-FIB SEM) images and Energy-Dispersive X-ray Spectroscopy (EDX) line scan data for cycled CS cathode before derivatization, after derivatization, and after solid sulfur removal.

The HUGS method is validated first: For Sample A and its GC method, due to the sample amount requirement, we modified the titration GC by increasing the sample size tenfold to quantify Li mass up to 8 mg (Figure S4a) with the same accuracy of up to  $10^{-7}$  g. Meanwhile, for Sample B and C's HPLC-UV analysis, a semi-preparative column was used for the first time instead of an analytical column to analyze sulfur-based species in the batteries, as shown in Figure S4b. This change allowed  $(\text{CH}_3)_2\text{S}_8$  (originally as  $\text{Li}_2\text{S}_8$  in the coin cell), which previously eluted very close to sulfur<sup>1-4</sup>, to be well separated from all other species. Additionally, with a 20-fold increase in injection amounts, the semi-preparative column provided double the temporal resolution and 20 times higher UV absorbance intensities. This allowed fractions collection with high quantities of relatively stable polysulfide species. For Sample B, its core reaction is the methylation of polysulfides. The methyl-terminated functional group can quench the conversion between polysulfides due to concentration changes during HPLC separation. To testify to the effectiveness of MeOTf in quenching the polysulfide conversion reaction, different concentrations of MeOTf-DME solutions (ranging from 0.11 to 0.44 M) were applied, as shown in Figure S4c. Variations in concentrations of the derivatized polysulfides are < 5%, suggesting the effectiveness of MeOTf in quenching polysulfide conversion reactions.

Moreover, according to previous studies, instability exists in methylated polysulfides, which can be mitigated by storing Sample B at 5°C. As shown in Supplementary Information, Figure S4d, storing Sample B at low temperature extends its stable time window from less than 24 hours to over one week, sufficient for completing HUGS testing. Moreover, To validate the effectiveness of sulfur removal during Sample B and C preparation, Cryogenic Focused Ion Beam Scanning Electron Microscopy (Cryo-FIB SEM) images and Energy-Dispersive X-ray Spectroscopy (EDX) line scans were performed to track the in-depth sulfur distribution in the cathode before and after MeOTf treatment (Sample B), and after DME mechanical shear force treatment (Sample C) (Figure S4e). The experiment was conducted under cryogenic conditions (< -170°C) to prevent ion beam/e-beam-induced sulfur sublimation. The results clearly show a reduction in sulfur signal on the surface after Sample B preparation, indicating the removal of  $\text{Li}_2\text{S}_x$  and  $\text{S}_{(\text{L})}$ , with only  $\text{S}_{(\text{S})}$  remaining in the cathode. After DME-shear force treatment, no sulfur signal was detected, indicating all  $\text{S}_{(\text{S})}$  dissolved in Sample C.

### 1.d. HPLC-UV Resolution Comparison

The resolution of elution was calculated to quantitatively assess the separation between the elution peaks of  $\text{Me}_2\text{S}_8$  and  $\text{S}_8$ . It is defined as the difference in retention times of the two peaks divided by the average of their peak widths.

$$R_s = \frac{2[t_{\text{Me}_2\text{S}_8} - t_{\text{S}_8}]}{W_{\text{Me}_2\text{S}_8} + W_{\text{S}_8}}$$

$t$  = Retention time

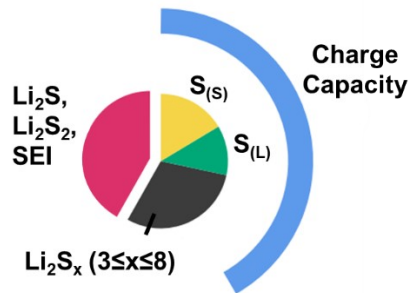
$W$  = Width of peak

**Table S3. Resolution parameters comparison between Semi-preparative and Analytical HPLC columns**

Parameters	Semi-Preparative Column	Analytical Column
$t(\text{Me}_2\text{S}_8)$	23.708	20.043
$t(\text{S}_8)$	25.376	21.252
$W(\text{Me}_2\text{S}_8)$	0.068	0.099
$W(\text{S}_8)$	0.081	0.088
$R_s$	22.39	12.93

**Table S4. Activity of the species in Li-S batteries at fully charged state**

















Activity	$\frac{1}{8}\text{S}_8$	$\frac{1}{8}\text{Li}_2\text{S}_8$	$\frac{1}{7}\text{Li}_2\text{S}_7$	$\frac{1}{6}\text{Li}_2\text{S}_6$	$\frac{1}{5}\text{Li}_2\text{S}_5$	$\frac{1}{4}\text{Li}_2\text{S}_4$	$\frac{1}{3}\text{Li}_2\text{S}_3$	$\frac{1}{2}\text{Li}_2\text{S}_2$	$\text{Li}_2\text{S}$
Active Portion	S	$\frac{7}{8}\text{S}$	$\frac{6}{7}\text{S}$	$\frac{5}{6}\text{S}$	$\frac{4}{5}\text{S}$	$\frac{3}{4}\text{S}$	$\frac{2}{3}\text{S}$	$\frac{1}{2}\text{S}$	0
Inactive Portion	0	$\frac{1}{8}\text{Li}_2\text{S}$	$\frac{1}{7}\text{Li}_2\text{S}$	$\frac{1}{6}\text{Li}_2\text{S}$	$\frac{1}{5}\text{Li}_2\text{S}$	$\frac{1}{4}\text{Li}_2\text{S}$	$\frac{1}{3}\text{Li}_2\text{S}$	$\frac{1}{2}\text{Li}_2\text{S}$	$\text{Li}_2\text{S}$






**Figure S5. HUGS capacity retention pie plot.**

**Table S5. Dataset comparing the HUGS method with other reported methods in the literature with references.**

Sr No	Publications	Method	Quantified Species (S, Li, polysulfides, radicals)	Detection Limits (ppb)	Tested Format (Electrolyte(0), Cathode(0.33), Coin(0.67), Pouch(1))	Marker
1	Current Work	HUGS	8	4.E+01	1	★
2	10.1149/2.060204jes	HPLC	0	1.E+07	0	●
3	10.1021/es049514e	HPLC	8	6.E+03	0	▲
4	10.1039/C4CP00958D	HPLC	9	1.E+07	0	■
5	10.1149/2.1011501jes	HPLC	1	4.E+03	0	◆
6	10.1002/cssc.201600878	HPLC	0	1.E+07	0	☆
7	10.1021/acsami.6b08904	HPLC	7	1.E+07	0	✚
8	10.1021/ac051854a	HPLC	6	2.E+01	0	✖
9	10.1016/j.electacta.2020.137227	HPLC	8	3.E+02	1	●
10	10.1002/aenm.201401888	HPLC	8	1.E+07	0	▼
11	10.1016/j.jpower.2013.01.132	HPLC	0	1.E+07	0	●
12	10.1039/D4JA00231H	HPLC	9	2.E+03	0	●
13	10.1071/EN14128	HPLC	6	2.E+04	0	●
14	10.1021/jasms.2c00113	HPLC	0	1.E+07	0	▶

15	10.1149/2.060204jes	ICP	1	1.E+07	0.67	
16	10.1016/j.jechem.2021.07.010	ICP	2	4.E+02	1	
17	10.1016/j.en-sm.2018.01.020	ICP	0	1.E+07	0	
18	10.1021/acs.jpcclett.6b00228	UV-Vis	0	1.E+07	0	
19	10.1149/1945-7111/ab8645	UV-Vis	3	3.E+05	0	
20	10.1021/ac2032244	UV-Vis	0	1.E+07	0.67	
21	10.1039/C4CP00958D	UV-Vis	0	1.E+07	0	
22	10.1149/1.1773733	UV-Vis	0	1.E+07	0	
23	10.1002/cssc.201402215	UV-Vis	0	3.E+05	0	
24	10.1021/jp5013208	UV-Vis	0	1.E+07	0	
25	10.1021/acs.jpcc.6b04264	UV-Vis	4	3.E+06	0	
26	10.1021/acs.iecr.1c04698	UV-Vis	5	1.E+07	0	
27	10.1246/cl.20486	UV-Vis	9	5.E+04	0	
28	10.1016/j.electacta.2019.04.119	UV-Vis	0	1.E+07	0	
29	10.1021/am5072942	Raman	0	1.E+07	0.33	
30	10.1002/cphc.201500448	Raman	0	1.E+07	0.67	

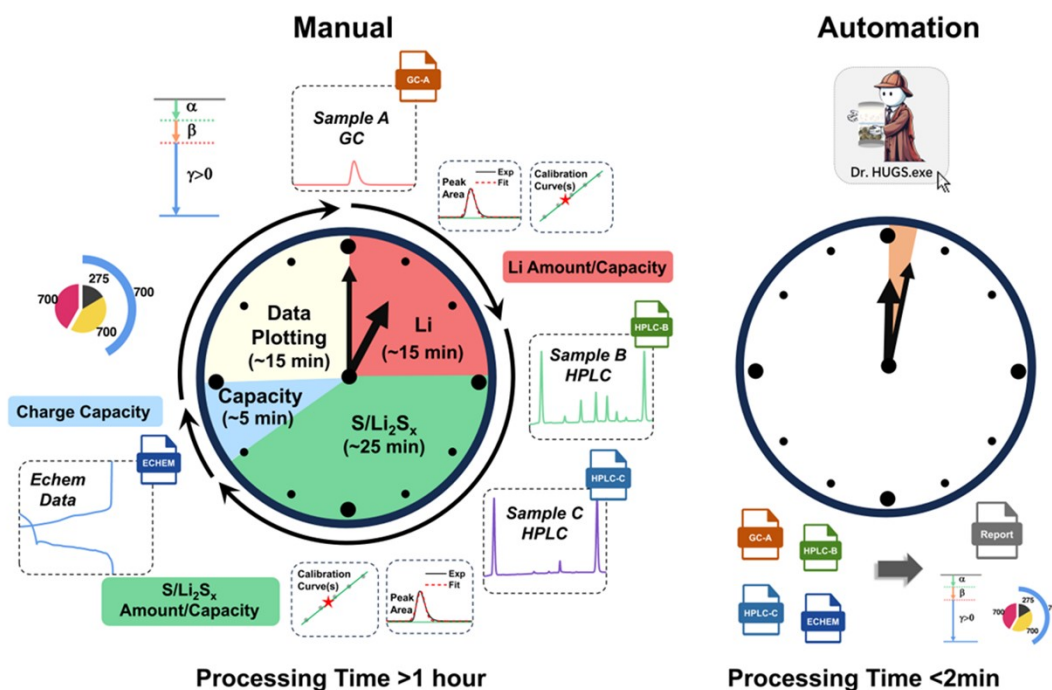
31	10.1002/ad mi.2016003 72	Raman	0	1.E+07	0.33	■
32	10.1021/cm 5044667	Raman	0	1.E+07	0.67	◆
33	10.1039/C6 SE00104A	Raman	0	1.E+07	0.67	★
34	10.1002/ani e.20160873 0	Raman	0	1.E+07	0.33	✚
35	10.1149/2.0 441805jes	Raman	0	1.E+07	0.67	✖
36	10.1002/cph c.20130097 2	NMR	5	1.E+07	0	●
37	10.1021/acs .jpcc.7b019 22	NMR	2	1.E+07	1	▲
38	10.1039/C4 CP00958D	NMR	0	1.E+07	0	■
39	10.1016/j.su sc.2014.07. 027	NMR	0	1.E+07	0.67	◆
40	10.1021/ja2 121926	TXM	0	1.E+07	0	●
41	10.1039/D0 TA12011A	XAS	0	1.E+07	0.67	●
42	10.1021/ja2 121926	XRD	2	1.E+07	0	●
43	10.1039/c4r a01388c	XRD	0	1.E+07	0.33	▲
44	10.1038/hen ergy.2017.6 9	XRD	4	1.E+07	0.67	■
45	10.1002/aen m.20150016 5	XRD	0	1.E+07	1	◆
46	10.1021/am 504763p	XRD	0	1.E+07	0.33	★
47	10.1021/jp5 00382s	Diffusion Coefficient	3	1.E+07	0	●

48	10.1149/2.0 851503jes	EPR	0	1.E+07	0	
49	10.1021/acs .jpcc.6b042 64	EPR	4	1.E+07	0	
50	10.1021/ac2 032244	ESR	0	1.E+07	0.67	

---

## 2. Dr. HUGS<sup>®</sup> Software

a



b

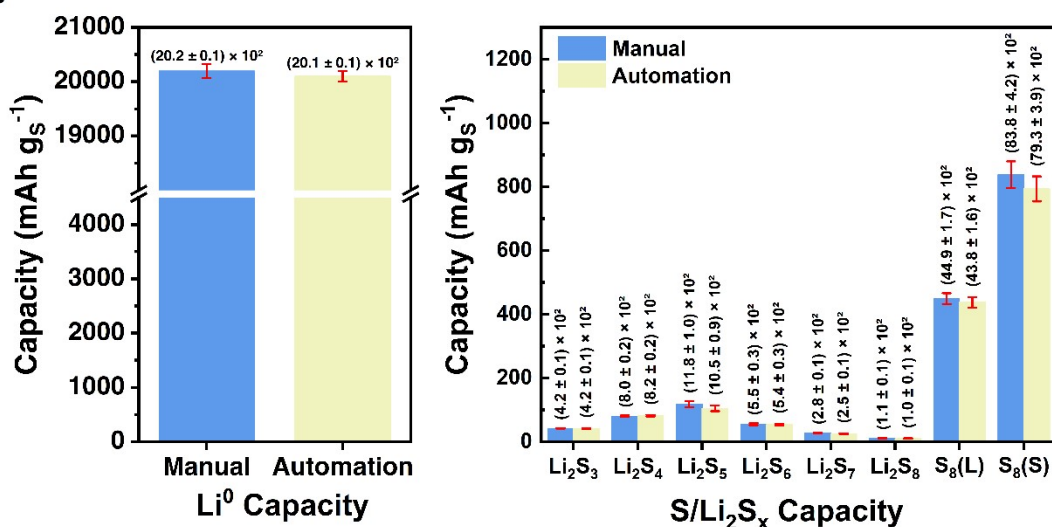


**Figure S6. Dr. HUGS<sup>®</sup> software for automated data processing of HUGS characterization.** **a.** workflow and estimated time of conventional data processing and automated data analysis using Dr. HUGS<sup>®</sup> software; **b.** Cross-validation of HUGS data between conventional processing and Dr. HUGS<sup>®</sup> automated analysis.

An interactive Python script based on the following packages was exported as an executable file.

```
import sys
import pandas as pd
import numpy as np
import textwrap
from scipy.optimize import curve_fit
from PyQt5.QtWidgets import (
    QApplication, QMainWindow, QLabel, QLineEdit, QPushButton, QVBoxLayout, QWidget,
    QComboBox, QFileDialog, QSpinBox, QHBoxLayout, QScrollArea, QSizePolicy
)
from PyQt5.QtGui import QPixmap, QImage, QPainter, QColor, QFont, QIcon
from PyQt5.QtCore import Qt
from matplotlib.backends.backend_qt5agg import FigureCanvasQTAgg as FigureCanvas
import matplotlib.pyplot as plt
import matplotlib.patches as patches
from matplotlib.patches import ConnectionPatch
from matplotlib.gridspec import GridSpec
from io import StringIO
from reportlab.lib.pagesizes import letter
from reportlab.pdfgen import canvas
from matplotlib.backends.backend_pdf import PdfPages
```

With a user-friendly GUI, the final product was designed which had the following functionalities and processes:

1. Importing the raw data files involving GC chromatograms, HPLC-UV chromatograms, and Electrochemistry Chem data. It also involved users inputting certain information regarding the battery, such as Pristine S and Li chip mass, SOC, TGC flask volume used, and dilutions made in HPLC sample preparation.
2. Calculate the areas for hydrogen gas peak from TGC chromatograms, areas of polysulfides and Sulfur from HPLC-UV chromatograms, and get charge capacity at the last step of cycling.
3. The code involved data processing to convert areas into concentrations and absolute species values based on calibration curves, then converting those values further into capacity equivalence.
4. The final part of the code involved an interactive window for producing HUGS capacity storage plots, vector plots, and system reports, defining the type of failure mechanisms, and data fitting done by the software for the user to look at. The figures can be exported separately or combined as a single PDF.



### 3. CS Cathode

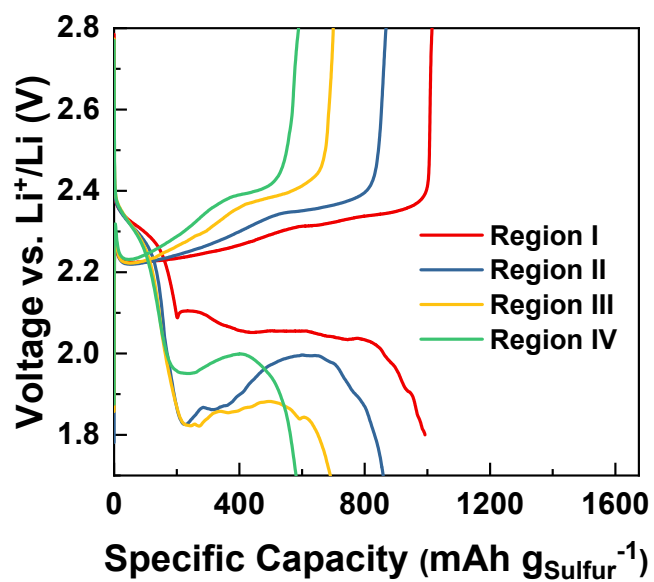


Figure S7. CS battery charge-discharge curves in different cycling regions.

### 3.a. Characterizations of CS

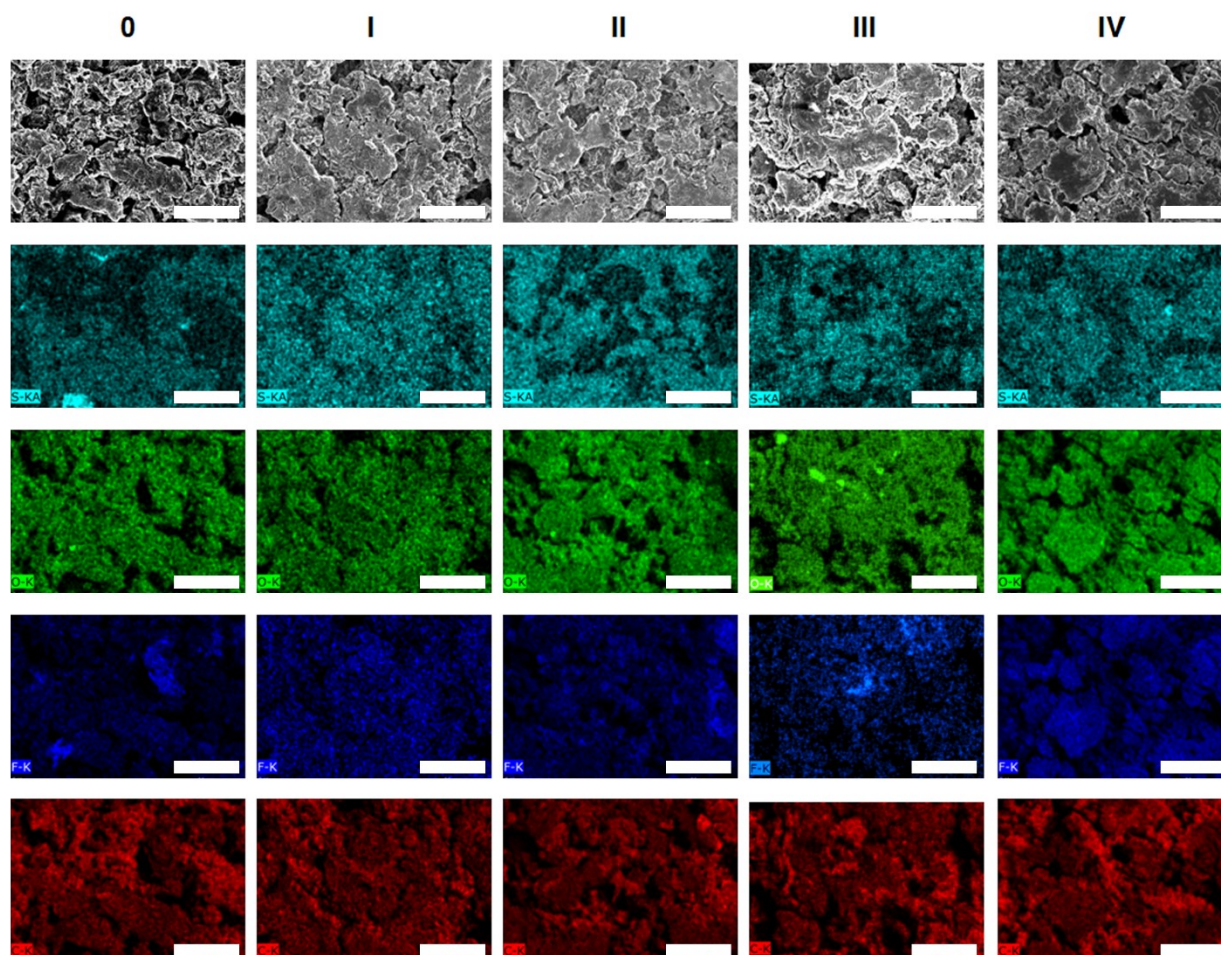
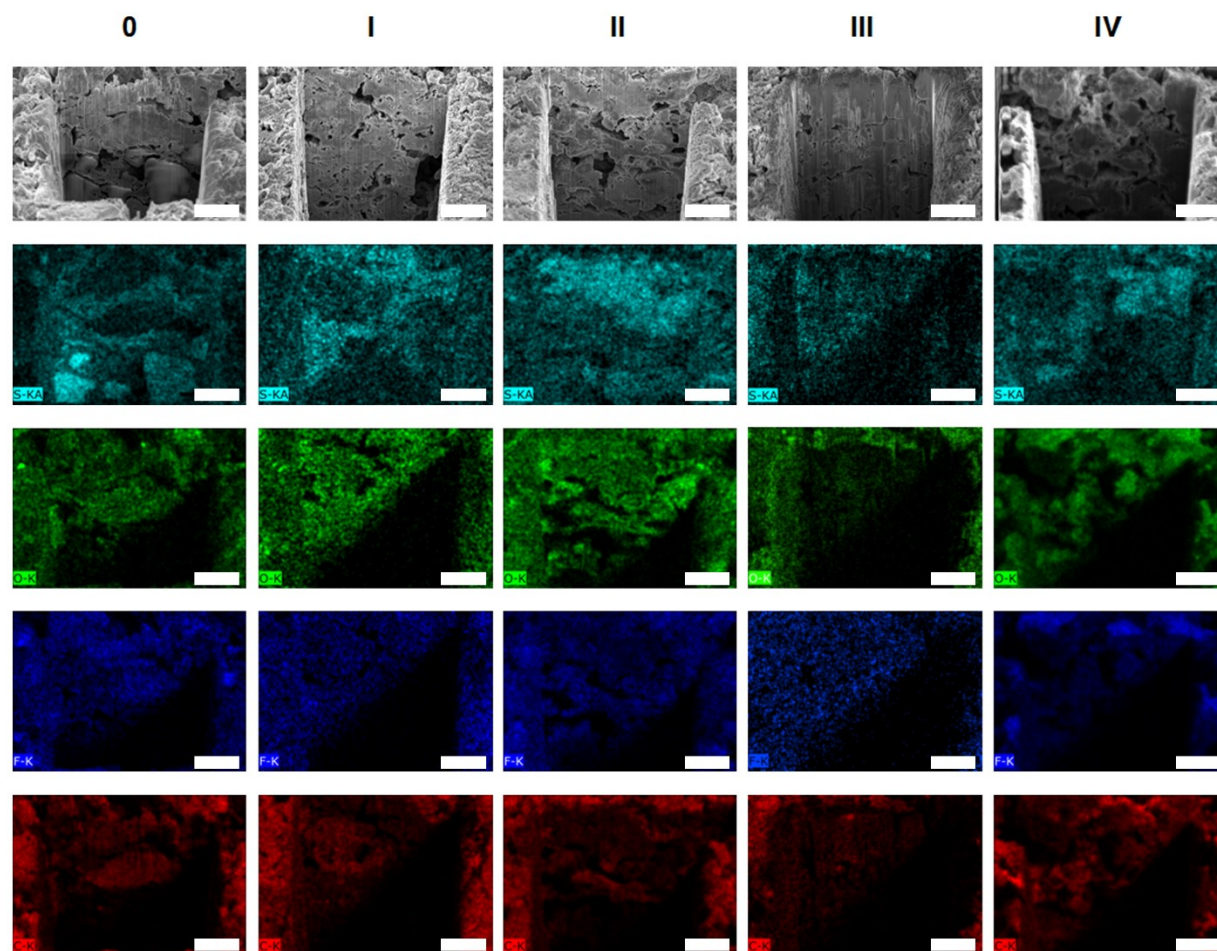
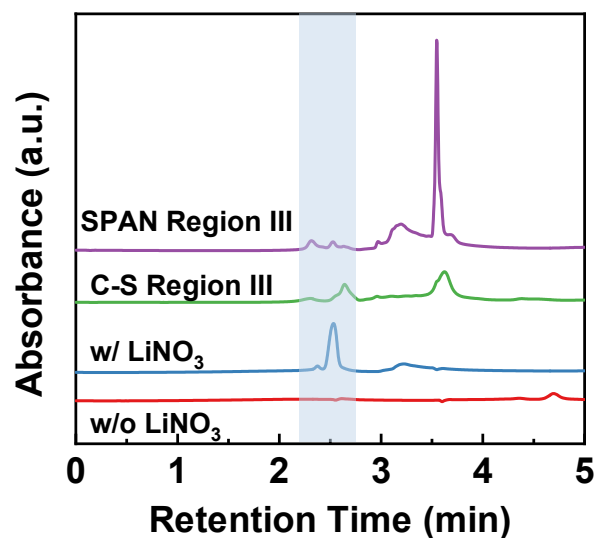


Figure S8. Cryo-FIB images and EDX mapping for cycled CS cathode top surface in different regions (Scale bar: 10 μm).



**Figure S9. Cryo-FIB SEM images and EDX mapping for the cross-section of C-S Cathodes in different cycling regions (Scale bar: 7  $\mu$ m).**



**Figure S10. LiNO<sub>3</sub> consumption is shown through HPLC-UV Chromatography.** The samples are as follows: Electrolyte without LiNO<sub>3</sub> (1M LiTFSI in DME: DOL (1:1 v/v)), Baseline electrolyte (1M LiTFSI in DME: DOL (1:1 v/v) + 2 wt.% LiNO<sub>3</sub>), CS and SPAN battery HUGS sample B in region III showing reduced intensity of LiNO<sub>3</sub> peak indicating its consumption.

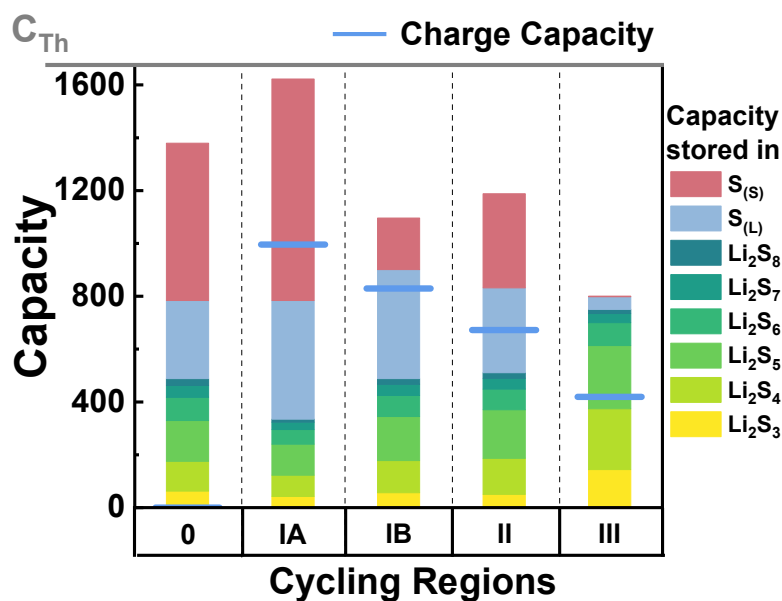


**Figure S11. CS HUGS capacity storage plot with each species.**

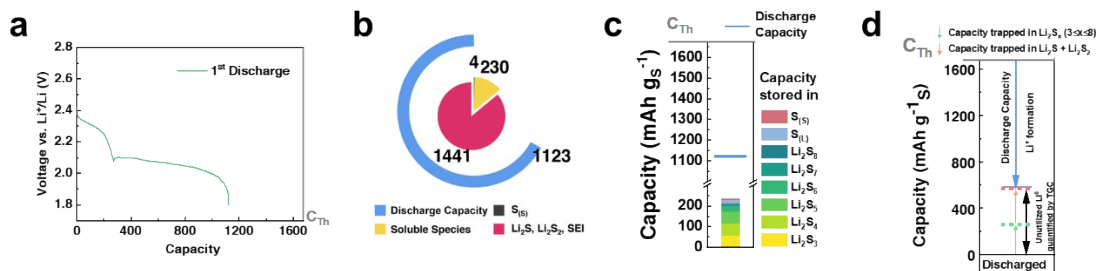


**Figure S12. CS battery at 1<sup>st</sup> discharge.** **a.** Discharge curve. **b.** HUGS capacity storage plot. **c.** HUGS capacity storage plot with each species. **d.** Capacity losses in the form of unutilized Li<sup>0</sup>.

### 3.b. Special cases in CS batteries

The cases are as follows.

**Baseline:** All conditions are the same as described in the study. The cell is cycled for 10 cycles, including formation.

**E/S = 6  $\mu$ L mg<sup>-1</sup>:** Electrolyte amount is reduced to 23  $\mu$ L from 38  $\mu$ L. The cell is cycled for 10 cycles, including formation.

**C/3:** The cycling rate after formation is increased from C/10 to C/3. The cell is cycled for 10 cycles, including formation.

**No LiNO<sub>3</sub>:** Instead of baseline electrolyte, 38  $\mu$ L of 1M LiTFSI in DME: DOL (1:1 v/v) is used, and as the cell could not be charged back, only one discharge and charge were performed. The charge capacity was equal to the theoretical charge capacity.

As seen in Figure S12c, the  $\beta$  vector increased in both low electrolyte and high C-rate cases. With less electrolyte, inactive Li ( $\gamma > 0$ ) remains the dominating cause of capacity loss while high C-rate more sulfide-rich SEI is supposed to form as  $\gamma$  is close to 0. No LiNO<sub>3</sub> is a special case tested to show that S(S) was absent on the cathode even if the battery is charged back to its theoretical limit. LiNO<sub>3</sub> plays a major sacrificial role in polysulfide converting back to Sulfur. In its absence, the Li loss due to liquid polysulfides was the highest ( $> 275$  mAh g<sup>-1</sup> equivalent) among all the batteries and conditions on which HUGS was performed in this study.



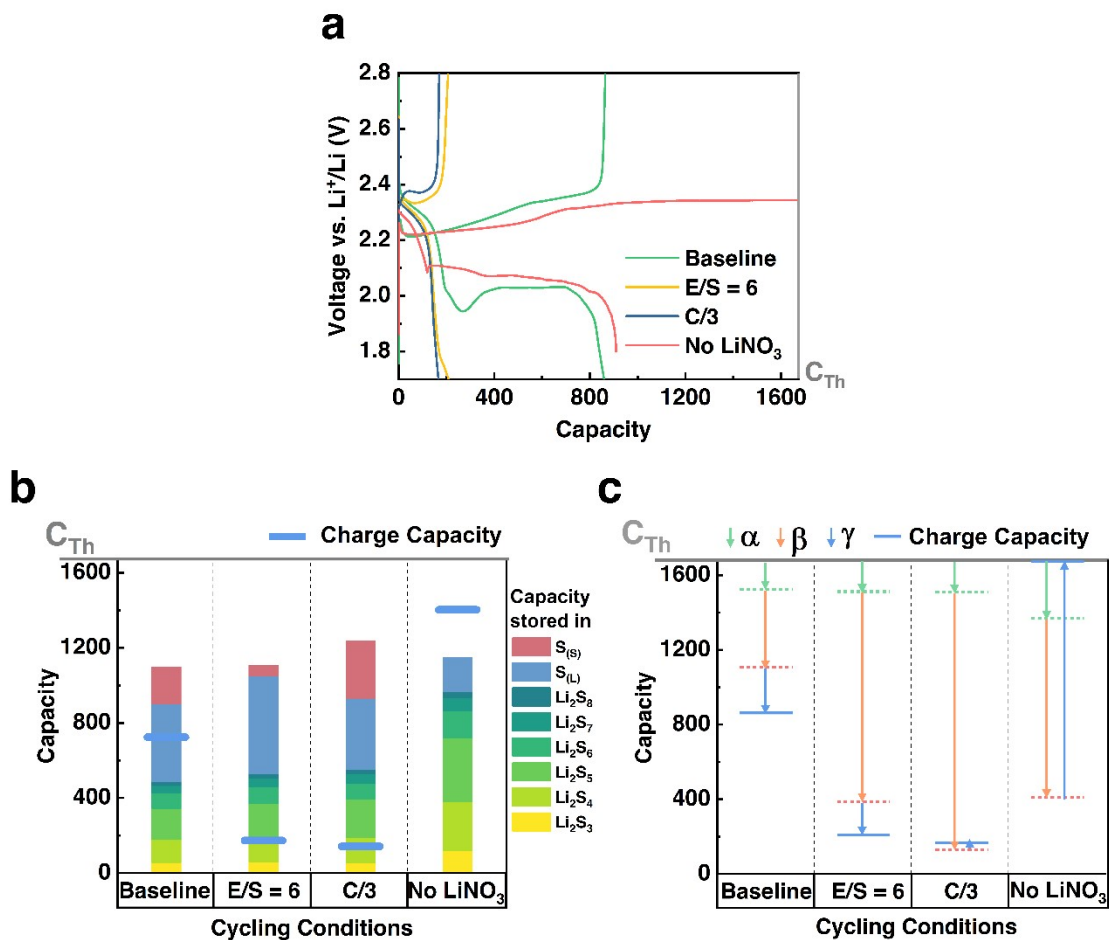


**Figure S13. HUGS analysis for CS cathode special cases. a.** Charge-discharge battery curves are available in each special case. **b.** Sulfur and polysulfide capacity retention in each special case. **c.** HUGS vector plots for each special case.

### 3.c. HATN cathode

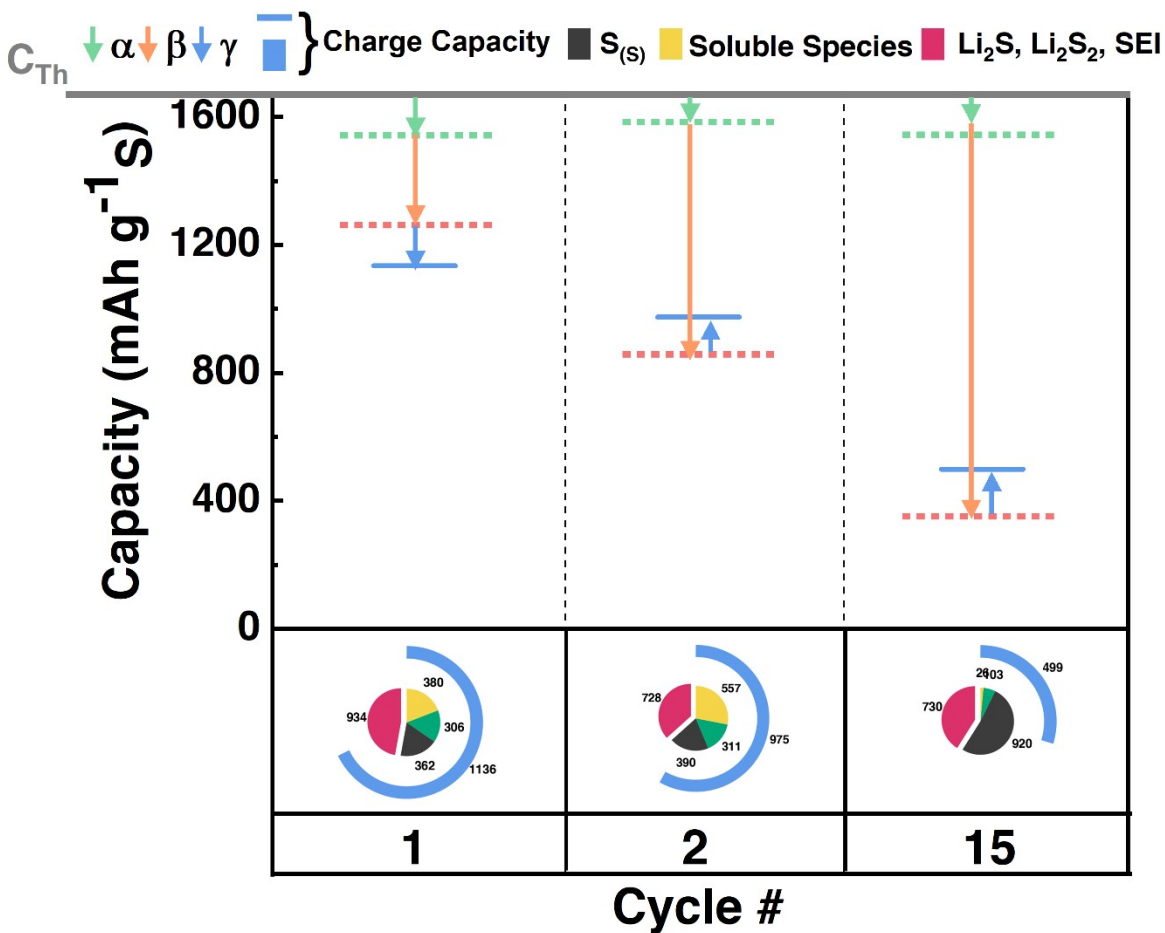


**Figure S14. HUGS analysis results for HATN cathode**

A previously reported HATN cathode<sup>5</sup> similar to CS was also tested to verify the HUGS method and look at the failure modes in HATN at different cycle numbers, which were inactivity of Li and S in the first cycle and mostly sulfide-rich SEI in later cycles.

### 3.d. CS Pouch Cells

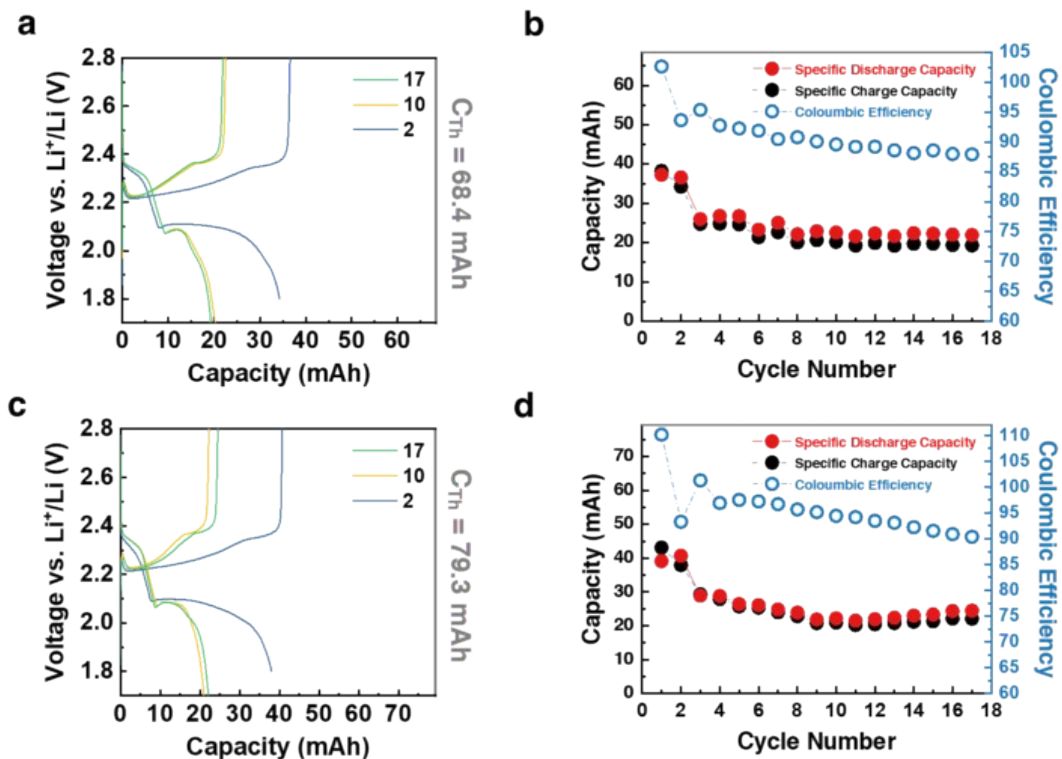


Figure S15. CS pouch cell charge-discharge curves and the cycling performance in (a-b) constant gap and (c-d) 30 psi constant pressure setups.

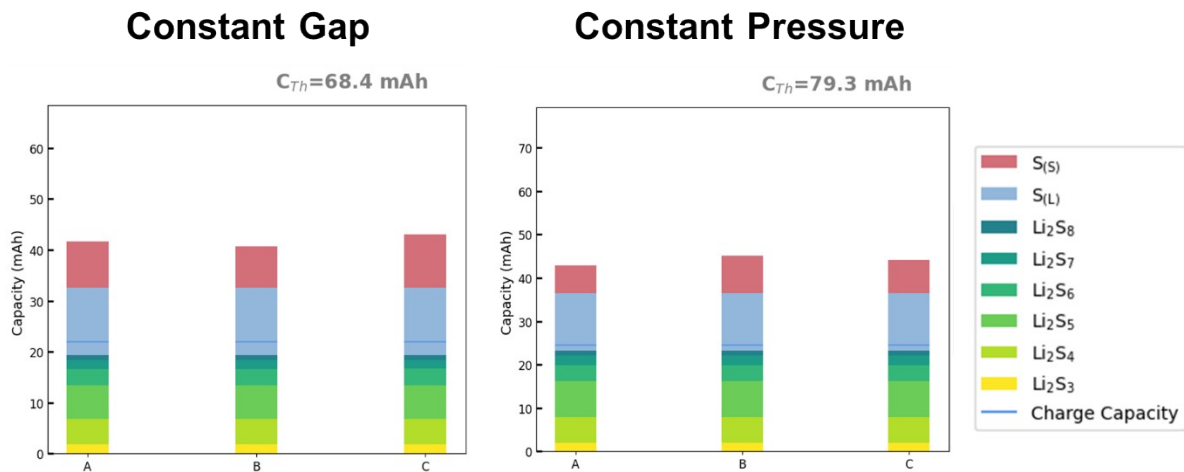
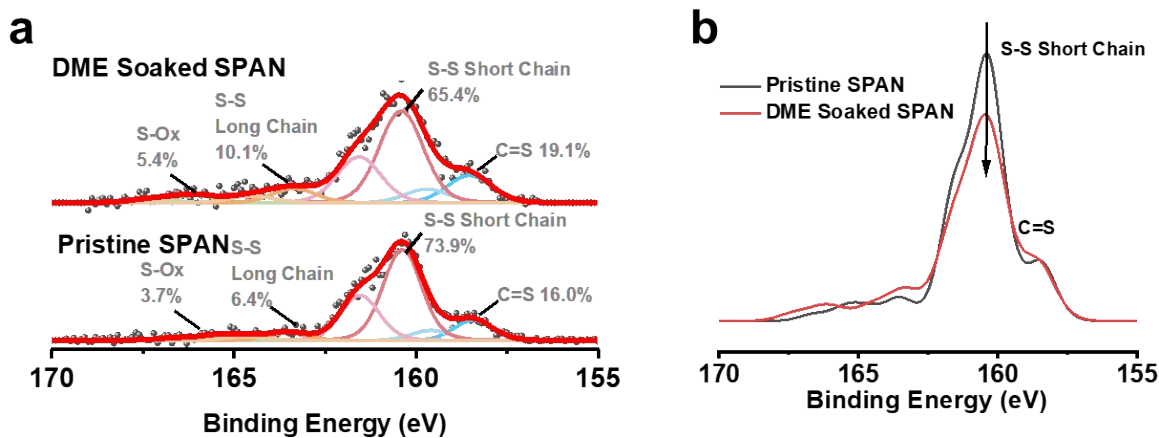


Figure S16. Pouch cell HUGS capacity storage plot with each species



## 4. SPAN

### 4.a. Characterizations of SPAN Cathode



**Figure S17. XPS analysis of SPAN cathode before and after soaking in DME.** (a) S 2p spectra with fitted components; peak assignments are based on Ref<sup>6</sup>. (b) S 2p spectra normalized to the C=S peak, showing a relative decrease in short-chain sulfur species after DME soaking.

The Raman spectra (Figure S18a) suggested that from Region 0 to Region I, the C-S and S-S bonding intensity decreased due to sulfur loss induced by the first discharge's irreversible capacity in SPAN. No further C-S or S-S intensity decay occurred from Region I to III. The cryo-FIB-SEM results (Figures S18b, S19, and S20) indicated minimal morphological changes across these regions. The relative EDX line scan results (Figure S18c) showed that sulfur content remained relatively stable, with only a <10% intensity drop observed in Region III. This indicates that polysulfide formation and shuttling are not SPAN's main drivers of performance degradation. On the anode side, XPS Li 1s and S 2p results suggested minimal polysulfide presence until Region III (Figure S18d).

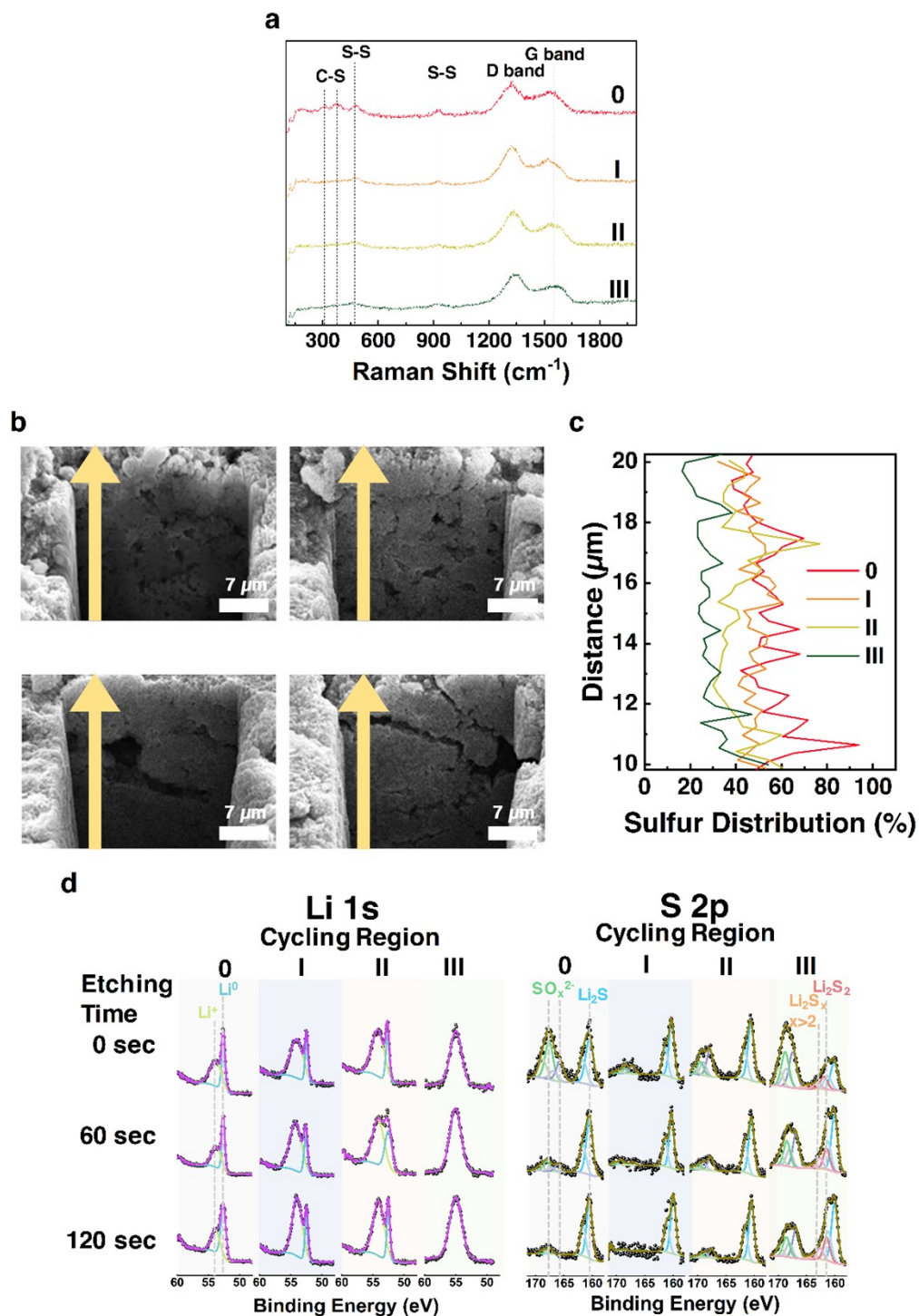


**Figure S18. Characterizations of Li-S Batteries with SPAN cathodes at Different Cycling Regions.** **a.** Raman spectra of cathodes. **b.** cryo-FIB-SEM images of cathode cross-section, and **c.** corresponding EDX Sulfur line scan. **d.** Depth profiling Li 1s and S 2p X-Ray photoelectron spectra (XPS) of anodes at different etching times.

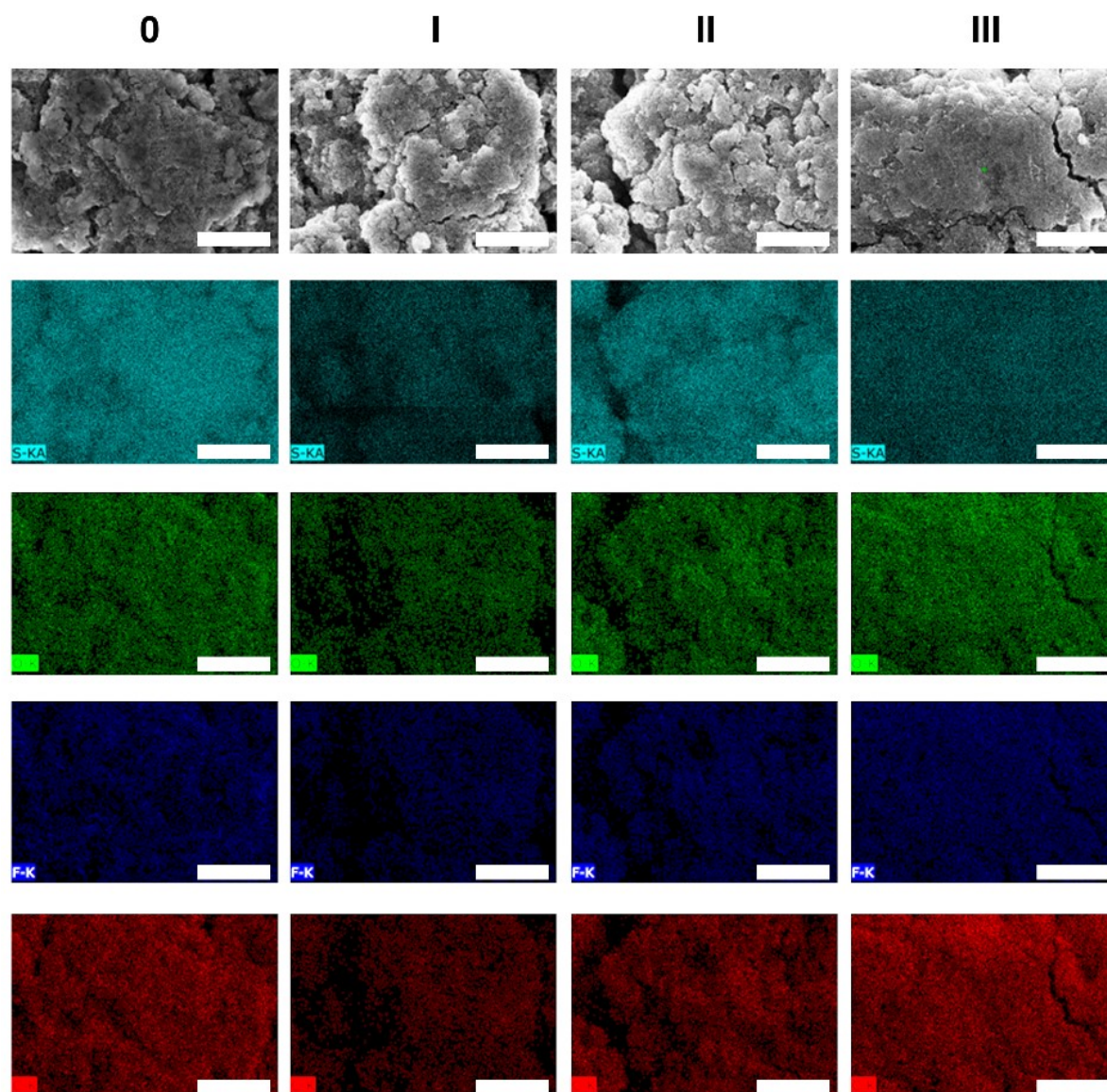


**Figure S19. Cryo-FIB images and EDX mapping for cycled SPAN cathode top surface in different regions (Scale bar: 20  $\mu\text{m}$ ).**



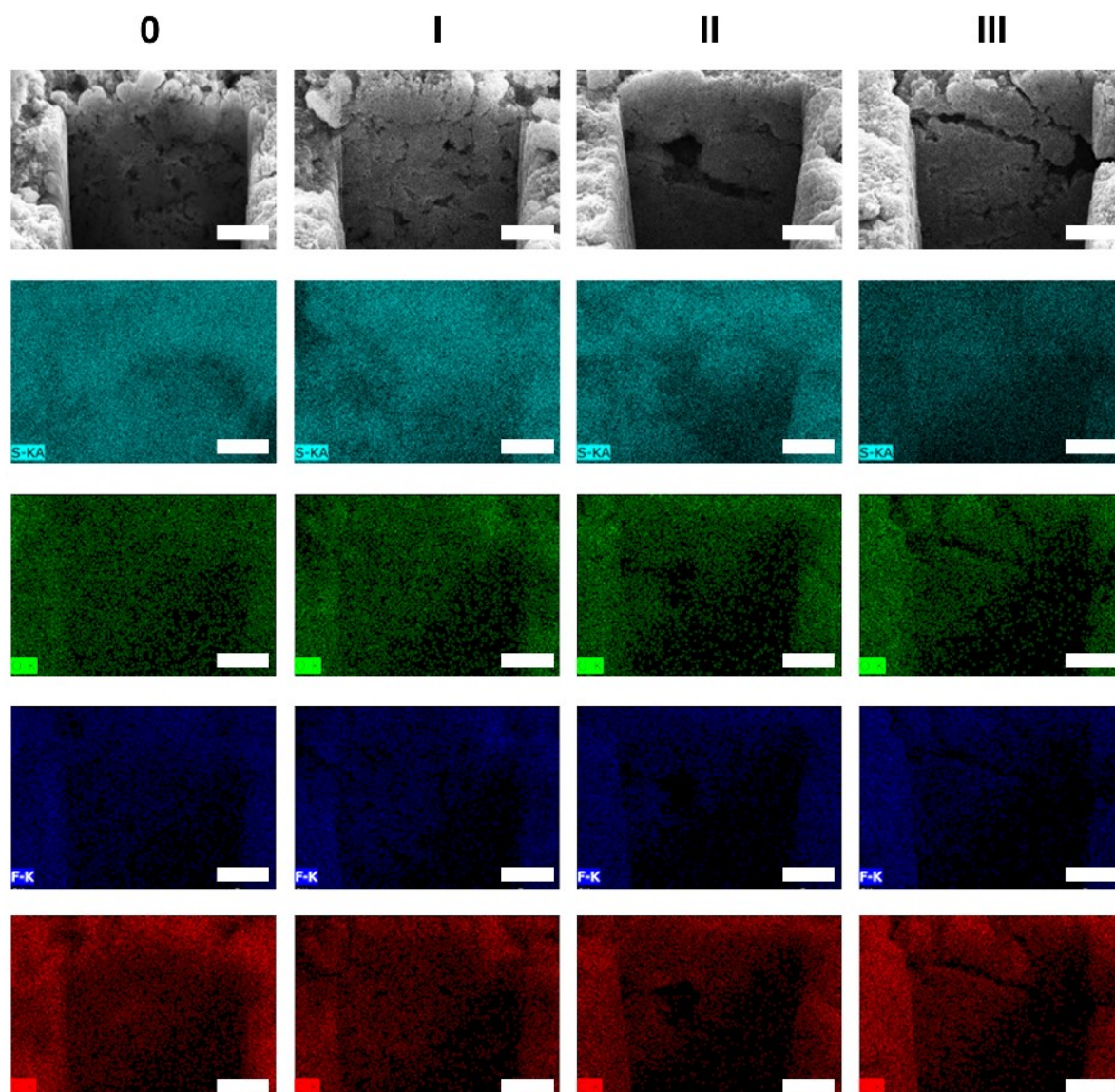


**Figure S20. Cryo-FIB SEM images and EDX mapping for the cross-section of SPAN Cathodes in different cycling regions (Scale bar: 7 μm).**

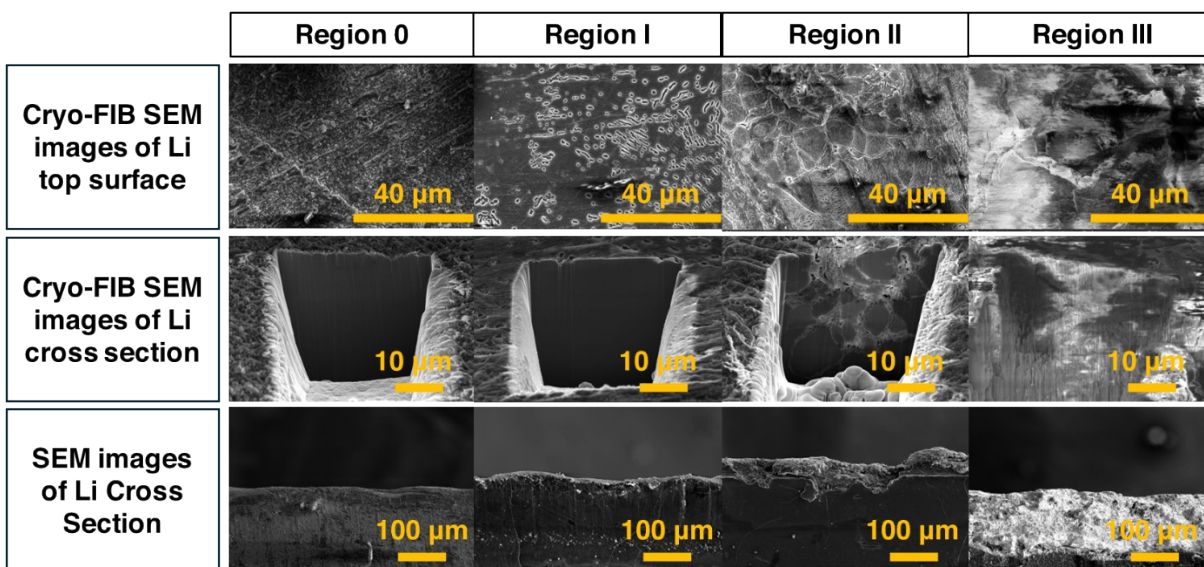


Figure S21. Cryo-FIB SEM top surface and cross-section images and SEM images of cross-section images of Li anodes from cycled SPAN batteries in different cycling regions.

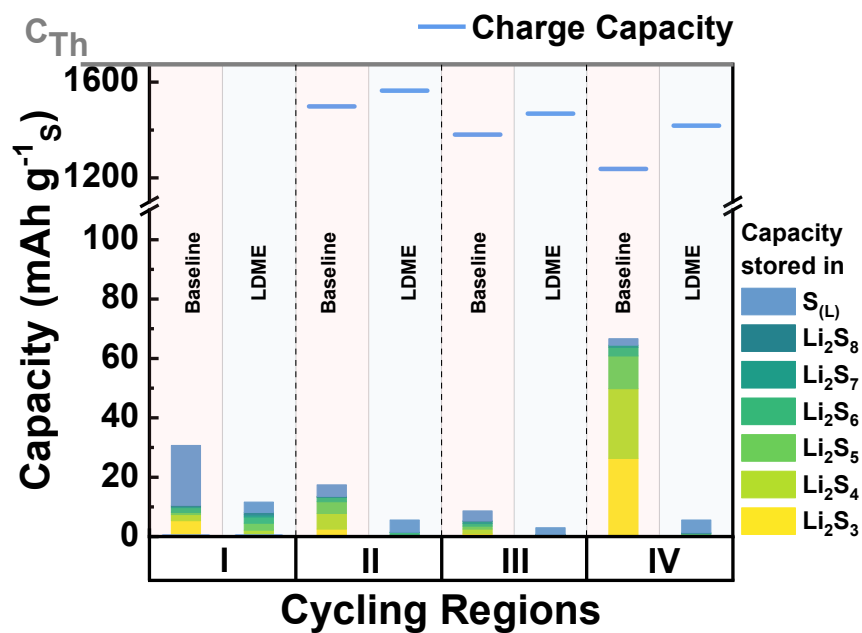
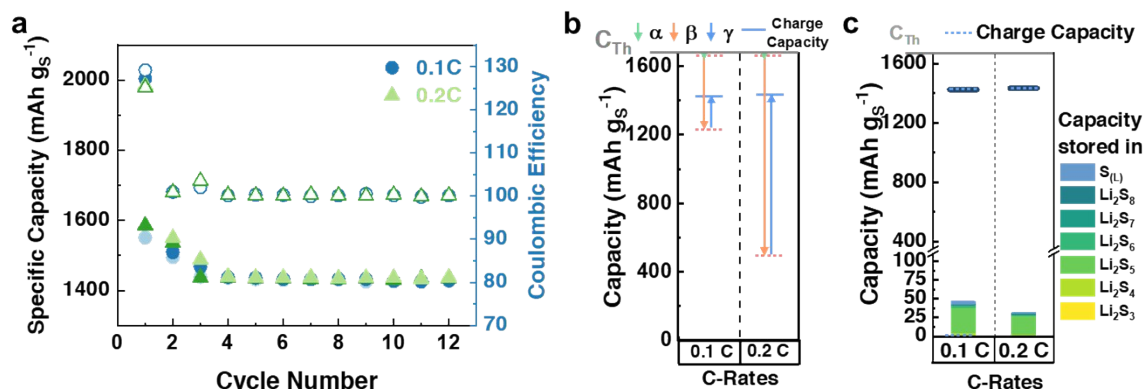


Figure S22. SPAN HUGS capacity storage plot with each species.

#### 4.b. Special Cases in SPAN batteries

**0.1C vs 0.2C-rate:** Li-SPAN batteries were made and cycled for 10 cycles at different C-rates after formation. 30 $\mu$ L of baseline electrolyte was used.



**Figure S23. HUGS analysis for Li-SPAN battery cycled at different C-rates. a.** Cycling performance. **b.** HUGS vector plot. **c.** HUGS capacity storage plot.

To understand how C-rate influences Li-metal losses and polysulfide distribution, batteries were cycled at two different C-rates (Figure S23a) and HUGS showed higher C-rate (0.2 C) had higher  $\beta$  vector or non-sulfide losses (Figure S23b). However, there was no significant difference in the amount of polysulfides generated (Figure S23c).

## References

- 1 D. Zheng, X. Zhang, C. Li, M. E. McKinnon, R. G. Sadok, D. Qu, X. Yu, H.-S. Lee, X.-Q. Yang and D. Qu, *J. Electrochem. Soc.*, 2015, **162**, A203–A206.
- 2 D. Zheng, X.-Q. Yang and D. Qu, *ChemSusChem*, 2016, **9**, 2348–2350.
- 3 D. Zheng, X. Zhang, J. Wang, D. Qu, X. Yang and D. Qu, *Journal of Power Sources*, 2016, **301**, 312–316.
- 4 D. Zheng, D. Liu, J. B. Harris, T. Ding, J. Si, S. Andrew, D. Qu, X.-Q. Yang and D. Qu, *ACS Appl. Mater. Interfaces*, 2017, **9**, 4326–4332.
- 5 X. Wang, Y. Yang, C. Lai, R. Li, H. Xu, D. H. S. Tan, K. Zhang, W. Yu, O. Fjeldberg, M. Lin, W. Tang, Y. S. Meng and K. P. Loh, *Angewandte Chemie International Edition*, 2021, **60**, 11359–11369.
- 6 S. Wang, B. Lu, D. Cheng, Z. Wu, S. Feng, M. Zhang, W. Li, Q. Miao, M. Patel, J. Feng, E. Hopkins, J. Zhou, S. Parab, B. Bhamwala, B. Liaw, Y. S. Meng and P. Liu, *J. Am. Chem. Soc.*, 2023, **145**, 9624–9633.